Bull. Mater. Sci. (2018) 41:60
https://doi.org/10.1007/s12034-018-1560-z

Magnetic measurements, Raman and infrared spectra of metal–ligand complex derived from $CoCl_2 \cdot 6H_2O$ and 2-benzoyl pyridine

S DATTA[1], A S MAHAPATRA[1], P SETT[2], M GHOSH[3], P K MALLICK[1] and P K CHAKRABARTI[1,*]
[1]SSRL, Department of Physics, Burdwan University, Burdwan 713104, India
[2]Physics Department, Gobordanga Hindu College, N. 24 Parganas 743273, India
[3]Spectroscopy Department, Indian Association for the Cultivation of Science, Kolkata 700033, India
*Author for correspondence (pabitra_c@hotmail.com)

MS received 30 March 2017; accepted 25 July 2017; published online 6 April 2018

Abstract. Nanocrystalline complex of $CoCl_2 \cdot 6H_2O-2$-benzoyl pyridine is prepared by chemical route. Each component of the desired complex is identified by analysing the X-ray diffractograms. Energy-dispersive X-ray analysis (EDX) data confirmed the presence of the desired elements of the sample. Theoretical optimized structure of the complex was derived using *ab initio* density functional level of theory (DFT) method of calculation. The average nanocrystallite size estimated from the XRD data is ∼43 nm. Static magnetic property of the complex is studied in the temperature range from 300 K down to 14 K. The estimated magnetic moment of the complex is high when compared to that of the free ion magnetic moment of Co^{2+} and this is attributed to the less effect of the crystal field acting on the ion in the organic complex due to which orbital moments are not fully quenched. The magnetic property of the complex is also remarkably enhanced compared to that of the diamagnetic 2-benzoyl pyridine which may be suitable for applications in devices. FTIR and Raman spectra of the ligand, 2-benzoyl pyridine and the synthesized complex are recorded at room temperature, which not only confirm the presence of each phase in the complex, but some interesting results are also extracted from the analyses of different Raman active modes of the complex.

Keywords. $CoCl_2-2$-benzoyl pyridine; magnetic property; Raman spectroscopy.

1. Introduction

Investigations of different physical and chemical properties of organic molecule-derived transition metal (TM) ion-based complexes have opened a wide research field in the interface of physics and chemistry [1–5]. The importance of TM ion coordinating suitable bridging ligands is appreciable in different physical, chemical and biological processes [6–10]. In the family of such complexes, different organic molecules can be considered, of which, aza aromatic and carbonyl compounds are of much interest for their certain elusive photophysical [11], photochemical [12] and biological [13] properties, which have attracted the attention of many research workers. Besides these, pyridine derivatives are very useful components in both the industry and biochemistry fields. Especially, benzoylpyridines are used as intermediates for pharmaceuticals and other organic syntheses [14]. Recent research works on the complexes obtained by the reaction of 2-benzoylpyridine (2-BOP) with manganese (II) and copper (II) cations provided interesting materials with new structural and magnetic features [15–18]. Reactivity of 2-BOP with manganese (II), nickel (II), copper (II) and NH_4SCN was studied by Malecki *et al* [19] and some studies of the complexes of 2-BOP with tin (II), manganese (II), nickel (II), copper (II) and cobalt (II) were reported by Plytzanopoulos *et al* [20].

In the above-mentioned works, the investigations like detailed analyses and studies of Raman spectroscopy, magnetic behaviour and their interpretation by using density functional level of theory (DFT) calculation, which normally provide precious information related to structural and thermophysical behaviour were not carried out. Considering this fact, here, in the present work, we have focussed our attention on the synthesis, detailed spectroscopic signatures and magnetic behaviour of the complex of $CoCl_2 \cdot 6H_2O-2$-benzoyl pyridine (henceforth designated as Co–2-BOP). The formation of the desired complex was confirmed by analysing the X-ray diffraction pattern. The structural feature of the complex was also confirmed by the *ab initio* DFT calculation. The Raman and FTIR spectra of 2-BOP and the synthesized complex were carried out to extract various useful informations related to structural changes occurring due to complexation. The structural morphology and the average particle size of the synthesized Co–2-BOP nanostructures were investigated using field emission scanning electron microscope (FESEM). Zero field-cooled (ZFC) magnetization and temperature-dependent static magnetic susceptibility of the complex were also measured to know the role of the cation in the magnetic property

as well as in bridging with the organic molecule in the complex.

2. Materials and methods

The complex of Co–2-BOP was synthesized by chemical method using $CoCl_2 \cdot 6H_2O$ and 2-BOP as precursor materials. 2-BOP and $CoCl_2 \cdot 6H_2O$ were separately dissolved in methanol kept in two beakers. Newly prepared solutions were sonicated for 1 h to obtain homogeneous solution of each precursor material. The solution of the organic ligand was then added drop-wise to the salt solution at room temperature (RT). The mixed solution was then stirred for 1 h. The homogeneous solution was covered by perforated paraffin paper for slow evaporation and the beaker containing the mixed solution was kept in a refrigerator at 15°C for about two weeks. Finally, small crystals of the desired complex were grown and these were collected from the dense solution. The collected crystals were dried at 40°C under vacuum. X-ray diffraction patterns of the individual component, $CoCl_2 \cdot 6H_2O$, 2-BOP and the prepared complex of Co–2-BOP were recorded by Brukers Advanced D8 difractometer with CuKα radiation ($\lambda = 0.15425$ nm) in the range of 2θ from 20 to 80°. FESEM observations were carried out by using a FEI Inspect-F50 SEM. Raman spectra of the samples were collected by J.Y. HORIBA, T 64000 system interfaced with a computer in the photon counting mode and fitted with an Ar+ ion laser using 488.0 and 514.5 nm as exciting wavelengths. The FTIR spectra of the complex were recorded on a previously calibrated Perkin-Elmer model 783 spectrophotometer. Magnetic measurements were carried out by a quantum design SQUID magnetometer.

3. Results and discussion

3.1 *XRD analysis*

X-ray diffraction (XRD) patterns of all the samples, 2-BOP, $CoCl_2 \cdot 6H_2O$ and the complex of Co–2-BOP are shown in figure 1a, b and c, respectively. To confirm the formation of the composite complex of Co–2-BOP, we have recorded the XRD pattern of each constituting component (2-BOP and $CoCl_2 \cdot 6H_2O$) as a reference. Here, 2-BOP was in polycrystalline phase. Sample of 2-BOP was obtained from Aldrich Chemical company, USA, with purity grade 98% and was used after checking its purity by HPLC. The XRD pattern of 2-BOP was taken as the standard pattern for the preparation of nanocomposite complex of Co–2-BOP. To substantiate this, we have also consulted the available JCPDS file (no. 13-0717) in this family, which shows that more-or-less all the peaks (except very few) are matched well with the observed peaks in figure 1a. All the peaks in the XRD pattern of figure 1b are matched very well with those of the desired phase of $CoCl_2 \cdot 6H_2O$ and the peaks are assigned by using the JCPDS file (no. 01-0173). The XRD patterns of the complex are shown in figure 1c and interestingly, all the peaks of $CoCl_2 \cdot 6H_2O$ and 2-BOP are also developed in this pattern. This fact confirmed the presence of each phase in the complex. It is to be mentioned here that in XRD pattern of the complex (figure 1c), some peaks of the $CoCl_2 \cdot 6H_2O$ and the ligand (2-BOP) are shifted with reference to those of their individual pattern. These slight shifts are attributed to the fact that the lattice strain in the composite state was changed. No additional peak is found in the nanocomposite state, which confirms the formation of the desired phase of the complex. The average crystallite size in the complex is calculated from the broadening of the most intensed peak by using the Debye–Scherrer equation,

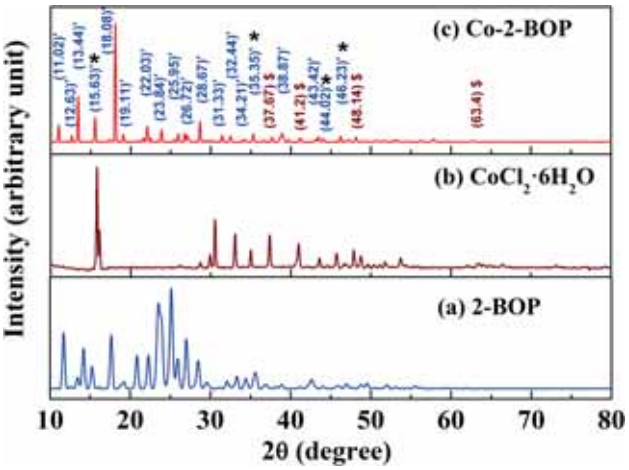

Figure 1. XRD patterns of: (**a**) 2-BOP, (**b**) $CoCl_2 \cdot 6H_2O$, (**c**) the complex Co–2-BOP ($' = 2-$BOP, \$ = $CoCl_2 \cdot 6H_2O$, * = common peaks of 2-BOP and $CoCl_2 \cdot 6H_2O$).

$$\langle D \rangle = 0.89\lambda/(\beta_{1/2}\cos\theta).$$

Here $\langle D \rangle$ is the average crystallite diameter, λ the wavelength of the incident X-ray radiation and θ the corresponding Braggs angle, $\beta_{1/2}$ is the full-width at half-maximum (FWHM) of the most intensed peak.

FESEM image (figure 2) confirms the formation of nanostructure of the Co–2-BOP complex. Different micrographs recorded during SEM observation are displayed in figure 2a and b. The nanoparticles in figure 2a are mostly spherical, but bigger size particles of different shapes are also seen in the other micrograph (figure 2 b). The estimation of average size from the displayed micrograph is difficult as particles of different sizes are found. Also, the scale is too high to measure the average size. But there are many small particles whose size is ∼50 nm, which confirmed the formation of the nanostructure of the complex. The crystallite size of $CoCl_2 \cdot 6H_2O$ and 2-BOP in pure form are respectively, 60 and 20 nm. The nanocrystallite size of the complex estimated from the XRD pattern is ∼43 nm. The bigger sized particles

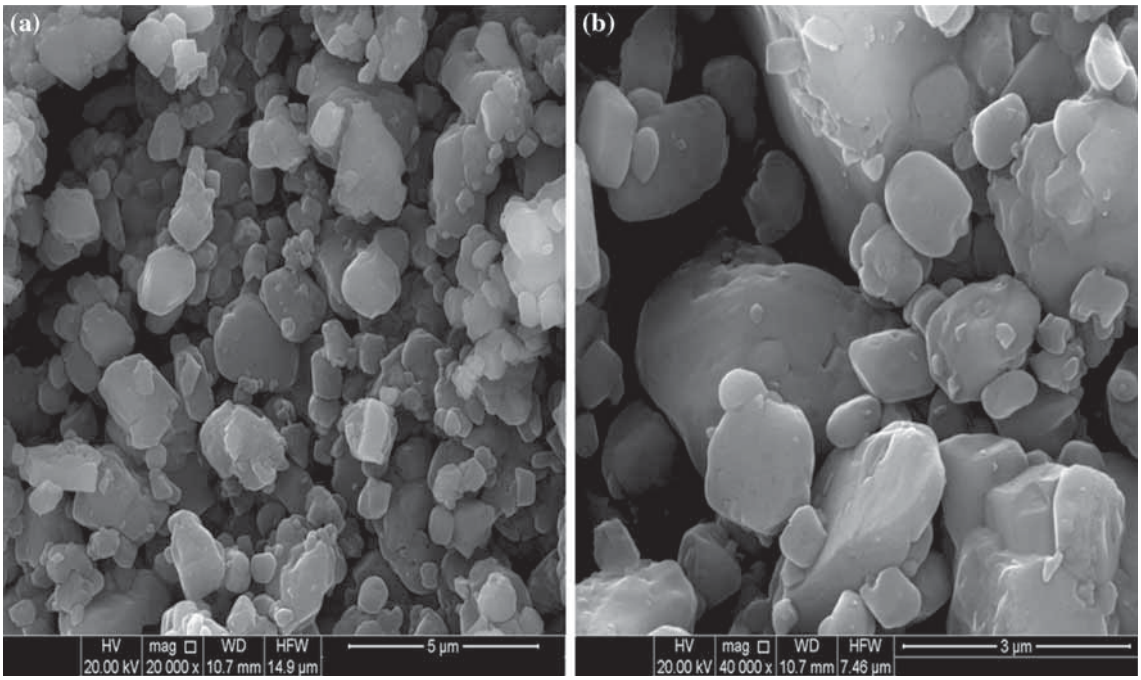

Figure 2. SEM image of the complex Co–2-BOP in (**a**) 5 and (**b**) 3 μm scale.

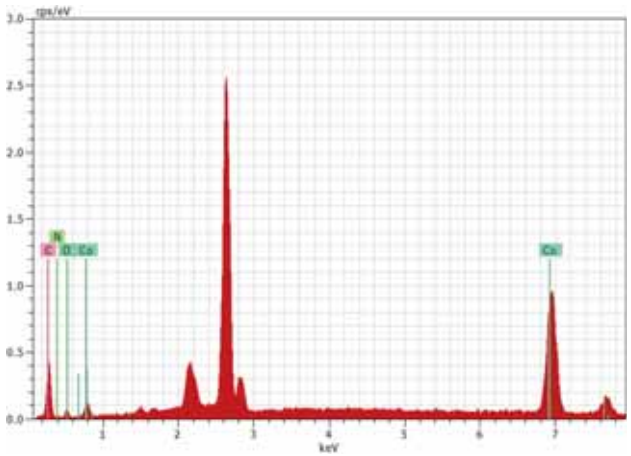

Figure 3. EDX spectra of Co–2-BOP.

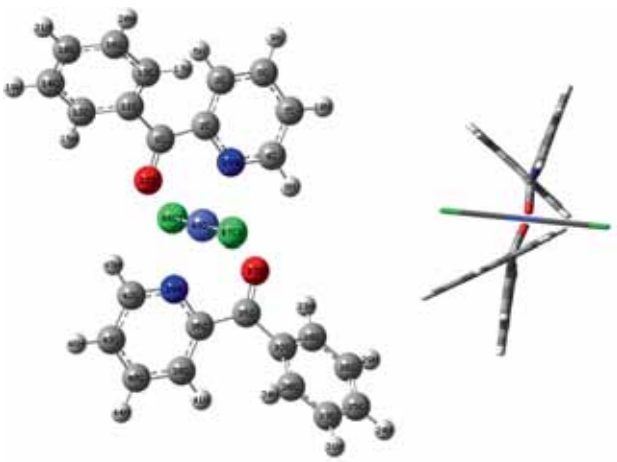

Figure 4. Optimized structural view obtained from *ab initio* DFT calculation of $CoCl_2$–2-benzoyl pyridine (Co–2-BOP) complex.

are quite likely in the micrographs due to the agglomeration of different particles in the complex. The elemental composition of the complex Co–2-BOP was confirmed by the EDX measurement and the corresponding results are shown in figure 3.

3.2 *Molecular geometry of Co–2-BOP*

The detailed structural view of the complex was achieved by *ab initio* DFT calculations. Using Gaussian 03 program package, theoretical calculations were performed by DFT using unrestricted B3LYP ((i.e., Becke three-hybrid exchange and Lee–Yang–Parr correlation functional (LYP)). The calculations of the system containing C, H, N, O and Cl centres were described by standard Pople split valance polarization basis set 6-31 + G(d,p), while for Co^{2+}-ion LanL2DZ was used. By allowing relaxation of all the parameters, a realistic optimized structure is obtained, which corresponds to true energy minimum. This optimized structure is shown in figure 4 and some selected values of the parameters of this structure are shown in table 1. The theoretically calculated structural parameters were compared with those obtained from the similar type of

studies of the ligand. Bond lengths and bond angles of the phenyl and pyridyl rings are in good agreement with those found in the structure of the ligand 2-BOP [22]. The structural features of the inner sphere of the metal ion point towards a distorted octahedral symmetry of the complex with the two chlorine atoms lying on the axial line. The angle between the two ring planes of the ligand in the complex is about 51° when compared to 60° in the free ligand [22]. The two rings are found slightly distorted and increased in size in the complex. Hence, also is the case of the carbonyl group, however, its planarity is maintained. Another interesting point is that the bond length between the carbonyl carbon and its nearest carbon atom of the pyridyl ring (1.489 Å) is found to be slightly greater than the corresponding entity (1.478 Å) of the phenyl ring, whereas in case of the free ligand, the former bond (1.517 Å) is significantly larger than the latter one (1.498 Å). In addition to this, it is also noticed that the C=O bond is larger in the complex (1.244 Å) than that of the ligand (1.213 Å). The increase in the carbonyl (C=O) and decrease in the $C_{carbonyl}$–$C_{C/N(ligand)}$ bond lengths are compatible with the observed interesting spectral features discussed in the Raman analysis of the complex.

Table 1. Equilibrium geometry of $CoCl_2-2$-BOP. (A) Bond lengths and bond angles in the geometry formed by cobalt ion with O, N and Cl atoms. (B) Selected bond lengths and bond angles of the ligand. (C) Bond lengths and bond angles of the carbonyl group.

(A)				
Bond length (Å)				
R_{CoO}	R(Co_{49}–O_{22})	2.172	R(Co_{49}–O_{37})	2.172
R_{CoN}	R(Co_{49}–N_{23})	1.993	R(Co_{49}–N_{39})	1.993
R_{CoCl}	R(Co_{49}–Cl_{44})	2.245	R(Co_{49}–Cl_{47})	2.215
Bond angle (°)				
A_{OCoN}	A(O_{22} Co_{49} N_{23})	78.008	A(O_{37} Co_{49} N_{39})	78.006
A_{OCoN}	A(O_{37} $Co_{49}N_{23}$)	102.00	A(O_{22} $Co_{49}N_{39}$)	102.00
A_{ClCoCl}	A($Cl_{47}Co_{49}$ Cl_{48})	179.97		
A_{NCoN}	A(N_{23} Co_{49} N_{39})	179.91		
A_{OCoO}	A(O_{22} Co_{49} O_{37})	176.39		
A_{NCoCl}	A(N_{23} Co_{49} Cl_{47})	89.95	A(N_{23} Co_{49} Cl_{48})	90.05
A_{NCoCl}	A(N_{39} Co_{49} Cl_{47})	89.96	A(N_{39} Co_{49} Cl_{48})	90.04
A_{OCoCl}	A(O_{22} Co_{49} Cl_{47})	91.83	A(O_{22} Co_{49} Cl_{48})	88.20
A_{OCoCl}	A(O_{37} Co_{49} Cl_{47})	91.78	A(O_{37} Co_{49} Cl_{48})	88.19

(B)

Bond length (Å)

	Ring I			Ring II		
	Co–2-BOP complex		2-BOP	Co–2-BOP complex		2-BOP
$R_{CC/CN}$	R(N_{23}–C_2)	1.357	(1.333)	R(C_{11}–C_{12})	1.429	(1.402)
	R(C_2–C_3)	1.395	(1.395)	R(C_{13}–C_{11})	1.401	(1.401)
	R(C_3–C_5)	1.400	(1.390)	R(C_{16}–C_{13})	1.398	(1.393)
	R(C_5–C_7)	1.391	(1.392)	R(C_{15}–C_{16})	1.417	(1.393)
	R(C_7–C_4)	1.401	(1.398)	R(C_{14}–C_{18})	1.395	(1.396)
	R(C_4–N_{23})	1.334	(1.339)	R(C_{12}–C_{14})	1.393	(1.388)
R_{CC}	R(C_2–C_1)	1.489	(1.517)	R(C_{11}–C_1)	1.478	(1.498)

Bond angle (°)

	Ring I			Ring II		
	Co–2-BOP complex		2-BOP	Co–2-BOP complex		2-BOP
$A_{CCC/CCN/CNC}$	A($N_{23}C_4C_7$)	121.45	(123.69)	A($C_{12}C_{14}C_{18}$)	119.53	(120.01)
	A($C_4C_7C_5$)	119.03	(118.30)	A($C_{14}C_{18}C_{16}$)	120.29	(120.01)
	A($C_7C_5C_3$)	119.05	(118.67)	A($C_{18}C_{16}C_{13}$)	120.54	(120.04)
	A($C_5C_3C_2$)	119.08	(118.64)	A($C_{16}C_{13}C_{11}$)	119.38	(120.31)
	A($C_3C_2N_{23}$)	120.89	(123.98)	A($C_{13}C_{11}C_{12}$)	119.76	(119.19)
A_{CCX}	A($N_{23}C_2C_1$)	113.80	(115.67)	A($C_{12}C_{11}C_1$)	117.51	(117.99)
	A($C_3C_2C_1$)	125.22	(121.18)	A($C_{13}C_{11}C_1$)	122.5	(122.76)

Table 1. (continued)

(C) Bond length (Å)			
		Co–2-BOP complex	2-BOP
R_{CO}	$R(C_1-O_{22})$	1.244	(1.213)
Bond angle (°)			
		Co–2-BOP complex	2-BOP
A_{CXC}	$A(C_2C_1C_{11})$	123.80	119.40
A_{CCO}	$A(C_2C_1O_{22})$	117.69	119.26
A_{CCO}	$A(C_{11}C_1O_{22})$	118.51	121.34

3.3 *Static magnetic properties*

To investigate the magnetic property of the nanocomposite complex of Co–2-BOP and also to estimate the valence state of the Co-cation in the complex, we have measured the magnetic susceptibility in the temperature range of 300–14 K. We have also measured the magnetic susceptibility of 2-BOP, which confirmed that 2-BOP is diamagnetic. But the magnetic susceptibility of the nanocomposite complex is comparatively high and the value of susceptibility at RT is 1.3045×10^{-5} emu g^{-1}. This observation clearly proves that the magnetic contribution of the complex arises due to the cobalt chloride part whose magnetic moment arises from the magnetic contribution of Co ions. The average value of the magnetic moment of the complex was estimated from the average molar susceptibility using the formula, $P_{\text{eff}} = 2.828(\chi_M T)^{0.5}$, ($\chi_M$ being the average molar susceptibility) and the calculated value of the magnetic moment at RT is 4.31 M_B (M_B being the Bohr magneton). We have calculated the magnetic moment of Co^{2+} ions in $CoCl_2$ using the equation $\sqrt{4S(S+1)}$ and the corresponding calculated value is 3.87 M_B. Here, no orbital contribution towards the magnetic moment was taken into account as the orbital components are normally quenched in the crystalline state. Thus, the calculated value of the magnetic moment obtained from the measured value of the susceptibility, at RT, is higher than the theoretically predicted value of the magnetic moment of the complex. The relatively high value of the magnetic moment suggests that orbital angular momentums of Co are not fully quenched in the environment of the complex. Thus, Co^{2+} ions are quite close to its free ion state. This observation also suggests that 2-BOP offers relatively lower binding with the Co^{2+} ion. Here, the ground state (^4F) of the Co^{2+} ion would split into two triplets and one singlet, where the triplet distribution of the level will depend on the crystal field. The population of the ions in these different crystal field levels will depend on the Boltzmann distribution law and the magnetic moment gets its contribution from these levels. The ground state of the ion has four-fold spin degeneracy and seven-fold orbital degeneracy. Thus, there is 28-fold degeneracy of the ground state. The DFT calculation suggests that the large distortion in the octahedral distribution due to which crystal field symmetry will be lowered. This will further split the degenerate levels and consequently the population will be redistributed. The ions will be populated among these levels and the susceptibility can be calculated from Van-Vleck expression, which will give the proper value of the magnetic moment. The present value suggests that most of the ions are populated in the higher states among the crystal field levels. Due to this fact, the free ion magnetic moment is modified, where different crystal field levels contribute to the magnetic moment according to their population.

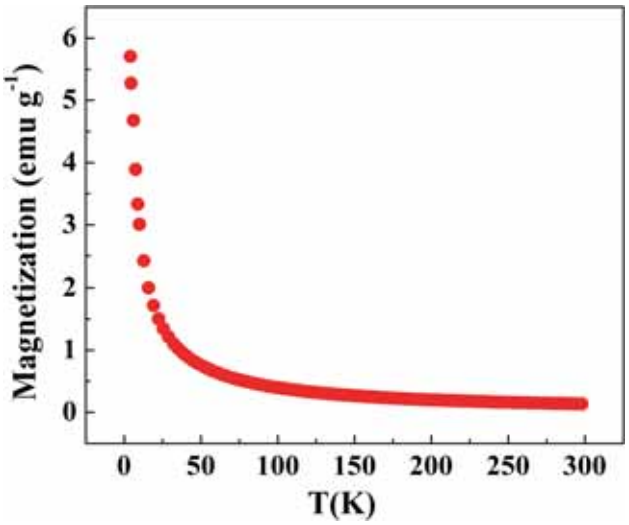

Figure 5. Thermal variation of magnetization recorded under zero field condition of the complex Co–2-BOP.

Thermal variation of magnetization recorded under zero field condition of the complex is shown in figure 5, from which it appears that the magnetization increases slowly with the lowering of temperature. To know the magnetic state and its transition, if any, in the measured temperature range (300–14 K), we have tried to fit the observed susceptibility *vs*. temperature curve of the complex by Curie–Weiss law, $\chi = C/(T-\theta)$, where C is the Curie constant and θ the Curie temperature. The thermal variation of the susceptibility

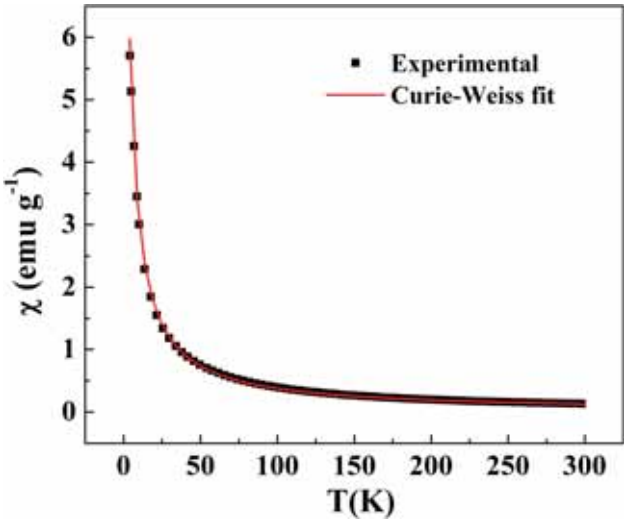

Figure 6. Thermal variation of the molar susceptibility of the complex Co–2-BOP.

of the complex including the Curie–Weiss fitting is shown in figure 6. It is clear that the susceptibility increases with the lowering of temperature. It is also evident from figure 6 that this law successfully fits the observed variation of susceptibility measured in the range of 300–14 K, which also indicates that the sample is paramagnetic in the entire range of temperature. The values of C and θ extracted from the Curie–Weiss fitting are 38.78 emu K mol^{-1} and –2.60 K, respectively. The negative value does not indicate the presence of any antiferromagnetic interaction of the Co-cations in the complex. This negative value of θ is mainly due to the crystal field effect, which is also found in different cases of our earlier studies [23,24].

3.4 *Raman analysis*

Raman and infrared spectra of the ligand (2-BOP) and the metal complex are shown in figures 7 and 8. From the

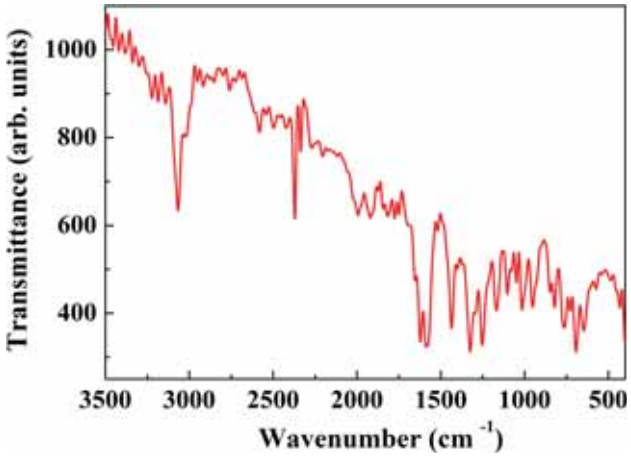

Figure 8. FTIR spectra of the complex of Co–2-BOP.

analyses of these spectra, some interesting things were observed when compared with the spectra of the free ligand (table 2). Firstly, the complex exhibits an overall diminution of Raman intensities with respect to the free ligand. When compared with the spectra of the free ligand [22], in the region below 600 cm^{-1}, the complex exhibits a number of new bands, both in the Raman and infrared spectra. Two such Raman bands are observed around 314, 326 cm^{-1} and these are assigned to the two ν(Co–Cl) stretching vibrations [20,25]. Besides these, the Raman spectra exhibit several other bands (in the said region), which cannot be matched with the ligand bands and their wavenumbers are around 360, 460, 485 and 536 cm^{-1}. The infrared spectra of the complex was recorded in the region above 400 cm^{-1} and some of the above bands in the Raman spectra were also observed in the infrared spectra. These bands, as shown in table 2, were assigned as the Co^{2+}-O/N stretching vibrations [22,25]. Some low frequency Raman bands are observed around 225 and below 200 cm^{-1}, which have been identified as the ligand–metal–ligand angle bending modes (table 2) [26]. Although, ν(C=O) vibration

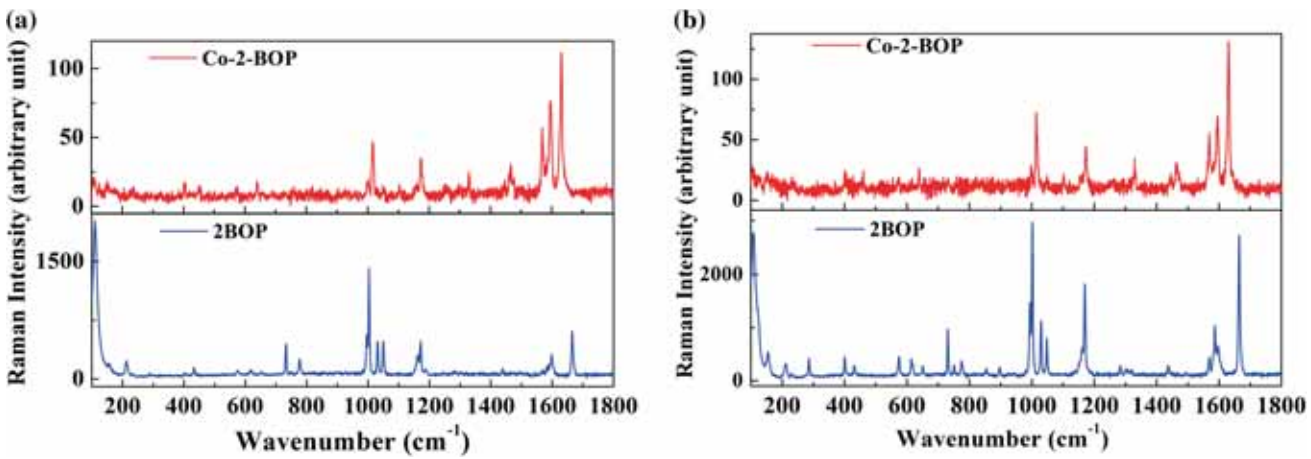

Figure 7. Raman spectra of the complex of Co–2-BOP and 2-BOP for excitation wavelengths of (**a**) 488.8 and (**b**) 514.5 nm.

Table 2. Raman and infrared spectra of 2-benzoyl pyridine and Co–2-BOP complex.

Excitation wavelength (514.4 nm)				Excitation wavelength (488.0 nm)				FTIR		
2-BOP (cm^{-1})	Intensity	Co–2-BOP (cm^{-1})	Intensity	2-BOP (cm^{-1})	Intensity	Co-2-BOP (cm^{-1})	Intensity	2-BOP (cm^{-1})	Co–2-BOP (cm^{-1})	Assignments*
		123	06			126	04			(X-Co-Y) angle bend
		145	10			144	06sh			(X-Co-Y) angle bend
155	506	153	13	157	203	153	08			CCx wag
		182	04			180	04br			(X-Co-Y) angle bend
211	320	204	10	214	232	205	03			CCx bend(I)
		223	05sh			227	03sh			(X-Co-Y) angle bend
231	134	232	10	229	112	235	08			CCx bend(II)
286	360	297	05	285	44	294	03			CC_X sym. stretch
		314	04			315	02			Co-Cl stretch
		329	07			326	05			Co-Cl stretch
		359	04			360	04			Co-O stretch
400	420	386	01wsh	401	58	385	03			Ring torsion(II)
400	420	401	12	410	50	405	12			Ring torsion(I)
431	273			432	152	433	04		433m	Ring torsion(I)
446	60	451	07			452	08		454w	Ring torsion(II)
		461	11			461	01		454w	Co-O stretch
		481	02			484	03		486wm	Co-N stretch
		538	02			536	02		539w	Co-N stretch
574	430	573	07	575	102	574	06		574m	CC_XC bending
614	363	616	07	617	102	616	03		607wbr	CCC ring bending(I)
650	235	640	16	652	88	639	13	650	649s	CCC ring bending(II)
(689)		687	06			689	04		693vs	Ring torsion (II)
731	936	731	10	733	437	732	04		728m	CCC ring bending (I)
751	250					760	05	750	766s	Ring torsion (I)
775	344			778	255	776	05			CH wag (I)

Table 2. (continued)

Excitation wavelength (514.4 nm)				Excitation wavelength (488.0 nm)				FTIR		
2-BOP (cm^{-1})	Intensity	Co–2-BOP (cm^{-1})	Intensity	2-BOP (cm^{-1})	Intensity	Co-2-BOP (cm^{-1})	Intensity	2-BOP (cm^{-1})	Co–2-BOP (cm^{-1})	Assignments*
(819)		818	06					(818)	822s	CxO wag
855	210			856	44	853	04br	856	848m	CH wag (II)
(896)						909	04	(896)	903wbr	CH wag (I)
925	67	922	03	928	44	922	06br		925sbr	CC stretch (II)
(943)		941	02			939	04			CH wag (II)
(962)						957	04		953vs	CH wag (II)
994	1424	998	18	995	507	1000	13	992		CCC ring bending(I)
1001	2912	1016	56	1002	1404	1016	38	1000	1016vs	CCC ring bending(II)
1029	1064	1031	03sh	1032	463	1029	01wsh	1026		CH bending(II)
1048	747	1051	08	1050	463	1051	08	1047	1051s	CC/CN stretch(I)
(1075)						1080	04	1075	1082w	CH bending(I)
1105	56	1101	10	1106	28	1104	12		1104s	CH bending(I)
1161	581	1157	10sh	1162	299	1158	10sh	1159	1167vs	CH bending(II)
1169	1796	1175	34	1171	476	1174	30	1168	1167vs	CH bending(II)
(1241)		1258	08			1257	06		1253vs	CC_X asymmetric stretch
1303	195	1296	08	1302	50	1297	06		1297w	CC stretch(II)
(1320)		1329	16			1329	13		1327vs	CH bending(II)
								(1401)	1400w	CC/CN stretch(I)
(1450)		1447	12			1447	08		1438vs	CC stretch(II)
(1465)		1465	23			1468	19			CC/CN stretch(I)
1490	110			1493	50	1476	07		1487w	CC stretch(II)
1568	354	1568	43	1568	98	1567	40		1576vsbr	CC/CN stretch(I)
1596	630	1595	60	1600	295	1596	65		1586vsbr	CC stretch (II)
1664	2665	1633	117	1666	613	1631	95		1623vs	C_XO stretch

Bracketed wavenumbers — ref. [22].

*Subscript X corresponds to carbonyl carbon and nonsubscripts X and Y correspond to pyridinic nitrogen and carbonyl oxygen.

appears as strong band both in the Raman and infrared spectra of the metal complex at 1630 and 1624 cm^{-1}, respectively, but the intensity of this Raman mode in the complex is much less than that of the free ligand. Significant down shift of wavenumber (of about 40 cm^{-1}) and reduction in intensity of this Raman band indicate electron donation from the metal ion to the antibonding orbital of the carbonyl group. This is compatible with the increase in bond length of C=O in the complex (1.244 Å) from the corresponding entity (1.213 Å) in the free ligand and also the corresponding decrease in bond lengths of the C_2– C_1/C_{11}–C_1 bonds (table 1). Some spectral shifts are observed in the spectra of the complex with respect to the free ligand. The modes around 1000 cm^{-1} exhibit some up-shifts. Specifically, the mode at 1016 cm^{-1} exhibits an up-shift of about 15 cm^{-1}. Another very interesting thing is that the modes around 297 and 1258 cm^{-1} are assigned as the CC_X symmetric and antisymmetric stretching vibrations and both these bands exhibit good amount of up-shifts (about 10 and 17 cm^{-1}), respectively, with reference to those of the free ligand [22]. These are compatible with the shortening of the $C_{carbonyl}$–$C_{x(pyridyl/phenyl)}$ bonds in the complex (table 1).

Since Raman and infrared spectra of the ligand were already analysed in detail [22], no elaborate discussion on the ligand modes is done here, only their assignments are shown in table 2 for comparison. Not only reduction of intensity, but some changes in the intensity pattern of the Raman bands are also observed in the complex. To be specific, two in plane CH bending modes at 1031 and 1157 cm^{-1} exhibit noticeable reduction in intensities relative to their adjacent band(s) in the metal complex compared to the free ligand spectra.

4. Conclusion

The complex of Co–2-BOP is successfully prepared by the combination of chemical method and the aqueous solution technique of crystal preparation. Crystallographic phase of the complex was confirmed by analysing the XRD pattern. The geometry of the complex was evaluated in DFT calculation and the extracted results are utilized to analyse the observed Raman and infrared spectra. Most of the observed peaks in the Raman spectra are successfully correlated with the bond lengths and bond angles between different constituting atoms of Co–2-BOP found in the DFT calculation. The magnetic property was introduced in the diamagnetic phase of 2-BOP by combining it with the relatively strong magnetic part of $CoCl_2 \cdot 6H_2O$ through the formation of a nanocrystalline complex. 2-BOP is an important compound, which has high potential for applications in different fields of industry. Thus, the introduction of magnetic property in the prepared complex may widen the scope of application in different fields of physics and chemistry. The observed value of magnetic moment is high when compared to that of the free ion magnetic moment, which suggests that orbital contribution was not completely quenched in the crystal field matrix of the Co–2-BOP. Also, this fact suggests that the freeness of the Co^{2+} ions in Co–2-BOP is more when compared to other crystalline system of transition metal ions where the orbital magnetic moment are fully quenched. This departure is attributed to the redistribution of Co^{2+} ion in different crystal field levels, where the magnetic moment gets its contribution from both spin and angular momentum states according to the population obtained from Boltzmann distribution. This view is also in good agreement with the observed Raman spectroscopic studies, where the presence of the valence state of Co^{2+} ion is also found.

Acknowledgements

We acknowledge the financial support received from DST, Govt. of India, through FIST program.

References

[1] Browne W R, Hage R and Vos J G 2006 *Coord. Chem. Rev.* **250** 1653
[2] Mautner F A, Louka F R, Le Guet T and Massoud S S 2009 *J. Mol. Struct*. **919** 196
[3] Kaim W and Sarkar B 2007 *Coord. Chem. Rev.* **251** 584
[4] Demandis K D, Hartshorn C M and Meyer T J 2001 *Chem. Rev.* **101** 2655
[5] Kaim W, Klein A and Glockle M 2000 *Acc. Chem. Res.* **33** 755
[6] Ward M D 1997 *Chem. Ind.* **16** 640
[7] Paul F and Lapinte C 1998 *Coord. Chem. Rev.* **431** 178
[8] Brunschwig B S and Sutin N 1999 *Coord. Chem. Rev.* **187** 233
[9] Bencini A, Ceotini I, Daul C A and Ferretti A 1999 *J. Am. Chem. Soc.* **121** 11418
[10] Solomon E I, Brunold T C, Davis M I, Kemsley J N, Lee S K, Lehnert N *et al* 2000 *Chem. Rev.* **100** 235
[11] Bugarevich D S, Kajimoto O and Hara K 1994 *J. Phys. Chem.* **98** 2278
[12] Jinguji M J, Hosako Y and Obi K 1979 *J. Phys. Chem.* **83** 2551
[13] Wensea G, Skalski B and Paszyc S 1991 *J. Photochem. Photobiol.* **57A** 279
[14] Sett P, Datta S and Mallick P K 2011 *J. Raman Spectrosc.* **42** 859
[15] Dey S, Sarkar S, Zangrando E, Evans H S, Sutter J P and Chattopadhyay P 2011 *Inorg. Chem. Acta* **367** 1
[16] Goher M A S and Mak T C W 1985 *Inorg. Chem. Acta* **99** 223
[17] Mak T C W and Goher M A S 1986 *Inorg. Chem. Acta* **115** 17
[18] Abu-Youssef M A M, Escular A, Gatteschi D, Goher M A S, Mautner F A and Vicente R 1999 *Inorg. Chem.* **38** 5716
[19] Malecki G, Machura B, Swithicka A and Kusz J 2011 *Polyhedron* **30** 410
[20] Plytzanopoulos M, Pneumatikakis G, Hadjiliadis N and Katakis D 1977 *J. Inorg. Nucli. Chem.* **39** 963
[21] Frisch M J *et al* 2003 *Gaussian 03: Revision B.03* (Pittsburgh, PA: Gaussian Inc.)
[22] Datta S, Sett P, Chowdhury J, Ghosh M and Mallick P K 2011 *J. Appl. Spectrosc.* **42** 1447

[23] Sarkar B J, Bandyopadhyay A, Mandal J, Deb A K and Chakbarti P K 2016 *J. Alloys Compd.* **656** 339
[24] Bandyopadhyay A, Sutradhar S, Sarkar B J, Deb A K and Chakbarti P K 2012 *Appl. Phys. Lett.* **100** 252411
[25] Nakamoto K 1997 *Infrared and Raman spectra of inorganic and coordination compounds* (New York: John Wiley & Sons Inc.) 5th edn
[26] Faulques E, Perry D I, Lott S, Zubkowski J D and Valente E J 1998 *Spectrochim. Acta* **54A** 869